Economic Geology
Vol. 97, 2002, pp. 385–398

Experimental Constraints on the Sulfide- and Chromite-Silicate Melt Partitioning Behavior of Rhenium and Platinum-Group Elements

PARISA SATTARI, JAMES M. BRENAN,†

Department of Geology, University of Toronto, Toronto, Canada M5S 3B1

INGO HORN,* AND WILLIAM F. MCDONOUGH**

Department of Earth and Planetary Sciences, Harvard University, Cambridge, Massachusetts 02138

Abstract

We investigate the origin of high platinum-group element (PGE) abundances associated with chromite-rich rocks by determining the relative partitioning of these elements between chromite- and sulfide-silicate liquids. Chromites were crystallized in the presence of immiscible sulfide and silicate melts in experiments at 1 GPa, producing a few, relatively large (20–50 μm) crystals, which were analyzed by laser ablation ICP-MS. Our results show that the PGE inventory of chromite and silicate melt produced in experiments is dominated by sulfide and/or alloy micronuggets and that the intrinsic PGE content of these phases is low (sub-ppm), despite high concentrations in coexisting sulfide liquid (i.e., up to alloy saturation). Lower bounds on minimum sulfide-silicate melt PGE partition coefficients (D_{PGE}) calculated from this data are 0.4 to 10×10^4, which are similar to values determined in previous studies, confirming the extreme fractionation of these elements into the sulfide phase. Rhenium, which was added to experiments in order to constrain Re-Os fractionation, is highly concentrated in sulfide liquid, present at low but uniform levels in silicate melt, and undetectable in chromite. Calculated sulfide-silicate melt D_{Re} are 3.3 to 5.2×10^4, and experiments yielded lower bounds for D_{Os}/D_{Re} of 3, indicating that sulfide-silicate melt equilibrium can fractionate Re from Os. Minimum sulfide melt-chromite partition coefficients are 1,000 or more, indicating that coexisting sulfide melt will be the dominant host for the PGE. Using this partitioning data, we have calculated the mass balance for Ir in chromite-sulfide mixtures and show that for rocks with greater than 200 ppm sulfur, less than 24 percent of the Ir will be in chromite, illustrating that chromite is not the significant PGE host even in low sulfur chromitites. In an experiment saturated in Ir-Re alloy, we measured a maximum iridium concentration in run-product chromites of 150 ppb, which, when combined with an estimate of the Ir activity in the coexisting alloy, yields a maximum Ir solubility of ~210 ppb. We have found examples of chromitites with Ir contents exceeding this value, indicating that these samples have accumulated an additional PGE-bearing phase. Such results support the notion that interstitial sulfide liquid, or accessory minerals included at the magmatic stage (i.e., laurite, alloys), are most likely to be the dominant primary hosts for PGE in chromite-rich rocks.

Introduction

THE IGNEOUS geochemistry of the platinum-group elements (PGE) has been extensively studied over the past several decades, yet the processes by which these elements are concentrated and fractionated from each other are poorly understood. At least five different phases have been proposed as playing an important role in affecting PGE behavior during melting and solidification: sulfide melt, PGE-rich sulfides or alloys, primary liquidus minerals such as olivine or chromite, and syn- to postmagmatic hydrothermal fluids (e.g., Barnes et al., 1985; Peach and Mathez, 1996). Data from both natural assemblages and experiments exist to at least partially evaluate the role of sulfides, alloys, and fluids on controlling both the absolute and relative PGE abundances in different mafic and/or ultramafic igneous rocks. However, observations to assess the role of primary liquidus phases such as olivine and chromite in PGE fractionation and concentration are few and yield ambiguous results (summarized below). In this paper, we document the partitioning behavior of Re and PGE between coexisting chromite- and sulfide-silicate melts with the specific intent of understanding the association of anomalously high PGE concentrations with chromitite segregations.

† Corresponding author's e-mail: brenan@geology.utoronto.ca

* Present address: Department of Inorganic Chemistry, ETH Zurich, Universitatstrasse 6, CH-8092 Zurich, Switzerland.

** Present address: Department of Geology, University of Maryland, College Park, Maryland 20742-4211.

Observational and Experimental Evidence for Chromite as a PGE Host

Various evidence has accumulated in support of the notion that chromite may be a significant host for the PGE in mafic and ultramafic igneous rocks. For example, analyses of mineral separates from ultramafic xenoliths collected at Kilbourne Hole, New Mexico, led Hart and Ravizza (1996) to suggest that Os is compatible in olivine and Cr-bearing spinel, with calculated mineral-silicate melt partition coefficients greater than 20. Moreover, Mitchell and Keays (1981) reported PGE abundances in whole rock and mineral separates from ultramafic xenoliths from various localities, which identified Cr-spinel, in addition to interstitial sulfide, as the significant PGE host. Further support for a PGE association with Cr-rich spinel or chromite comes from the correlation between Ir and Cr in various members of the Fiskenaesset Complex (West Greenland; Morgan et al., 1976) and mafic and/or ultramafic lavas (Hamlyn et al., 1985; Crocket and MacRae, 1986; Brügmann et al., 1987), as summarized by Peach and Mathez (1996). In addition, cumulate chromitites from different igneous settings, such as those in layered

intrusions, ophiolites, and alpine-type peridotites, are known for their anomalously elevated PGE levels (McLaren and DeVilliers, 1982; Page et al., 1982; Talkington and Lipin, 1986; Peck and Keays, 1990, Peck et al., 1992; Von Gruenewaldt and Merkle, 1995; Zhou et al., 1998). Indeed, earth's richest PGE ores are associated with chromitites in layered intrusions (Naldrett, 1981) such as the UG2 horizon of the Bushveld (McLaren and DeVilliers, 1982). An additional distinctive aspect of cumulate chromitites is their highly fractionated PGE abundances: chromitites from layered intrusions having elevated PPGE (Rh, Pt, Pd) relative to IPGE (Os, Ir, Ru), whereas the opposite is true for ophiolite-hosted chromitites. In addition to observations of natural materials, results of previous experimental studies have suggested that spinel-structured minerals may selectively concentrate some PGE. Specifically, Capobianco and Drake (1990) and Capobianco et al. (1994) measured spinel- and magnetite-silicate melt partition coefficients for Rh, Ru, and Pd at 1 bar (10^5 Pa), 1,275° to 1,450°C, and relatively high oxygen fugacities (i.e., FMQ + 1 to FMQ + 7), with their work revealing large partition coefficients for Ru (~20 to >4,000) and Rh (~80–300), and uniformly low values for Pd (i.e., <1). A notable aspect of these results is that partition coefficients for Ru are comparable to values measured between immiscible sulfide and silicate melts. As a consequence of this partitioning data, Capobianco et al. (1994) have suggested that other spinel group minerals, like chromite, may have a similarly selective affinity for the PGE, this accounting for the chromitite-PGE association.

Despite the evidence supporting the possible role of chromite in concentrating and fractionating the PGE, there also exists observational and analytical data that counter this notion. For example, Lorand et al. (1998) determined the PGE concentrations in a suite of orogenic lherzolites from the North Pyrenean Metamorphic zone and found no correlation between PGE content and Cr-spinel abundance. There was, however, a systematic positive correlation between PGE and sulfur content, reflecting the control of accessory sulfide minerals. With the exception of a weak trend in the Upper Critical zone, Maier and Barnes (1999) found no systematic correlation between whole-rock Cr and PGE content in rocks from the western Bushveld Complex, consistent with similar observations made for chromite-bearing rocks in ophiolites (e.g., Bacuta et al., 1990; Yang et al., 1995; Zhou et al., 1998). Most recently, Ballhaus and Sylvester (2000) used laser ablation ICP-MS to measure the PGE content of the various phases comprising the Merensky reef (Bushveld Complex) and found less than ~10 ppb PGE in chromite, whereas bulk-rock PGE abundances (ppm levels) could be adequately accommodated in coexisting pyrrhotite, pentlandite, and Pt alloy.

It is thus unclear as to whether chromite is a mineral that can dissolve considerable levels of PGE during initial growth, but that this inventory is partially or completed sequestered by subsolidus phases, or simply that chromite is coprecipitated at the magmatic stage with PGE-rich sulfide melt or PGE-bearing accessory minerals. Indeed, even in the Bushveld Complex, which is arguably the world's best characterized PGE deposit, the primary PGE concentration mechanism of the sulfide-bearing chromitites is still much debated (cf. Cawthorn, 1999). Thus, to assess whether chromite can be a significant host for the PGE requires knowledge of the chromite-silicate melt partition coefficients for these elements. Of equal importance, however, is evaluating the relative partitioning of PGE between chromite and sulfide melt, as this data is necessary to assess which of these phases will be important PGE hosts in sulfide-saturated systems. To this end, we have conducted experiments at high pressure (P) and temperature (T) to measure PGE (and Re) partitioning in samples that are saturated in chromite- and silicate- sulfide melt at an f_{O_2} relevant to basalt petrogenesis. This paper reports on our initial results in this endeavor, and we show that the PGE inventory of chromite and silicate melt produced in experiments is dominated by sulfide and/or alloy micronuggets, and that the intrinsic PGE content of these phases is low (sub-ppm), despite high concentrations in coexisting sulfide liquid (i.e., up to alloy saturation). Such results support the notion that interstitial sulfide liquid, or accessory minerals included at the magmatic stage (i.e., laurite, alloys), are most likely to be the dominant primary hosts for PGE in chromite-rich rocks.

Experimental Technique

Overview

Accurate characterization of the partitioning behavior of the siderophile elements presents specific analytical and experimental challenges. First, these elements typically exhibit low solubility in silicate melts (ppb levels; e.g., O'Neill et al., 1995; Borisov and Palme, 1997; Ertel et al., 1999), even at relatively high oxygen fugacities, making their detection in run-product phases difficult. Second, in experiments run at low f_{O_2}, Ertel et al. (1999) observed a marked decrease in Pt and Rh solubilities as a function of run duration, and the presence of submicron-scale Pt and Rh heterogeneities during LA-ICP-MS analysis. Their results suggest that PGE alloy nuggets remain dispersed in experimental melts for long periods of time, thereby making intrinsic melt concentrations difficult to measure and providing nucleation sites that become inclusions in growing phenocrysts. Finally, rhenium, which was added to experiments to better constrain Re-Os fractionation, is highly volatile at oxygen fugacities exceeding the iron-wustite buffer, (e.g., Borisov and Jones, 2000), ruling out 1 bar (10^5 Pa) experiments where control of f_{O_2} is by gas mixing.

To better assess the contribution of micronuggets to the apparent PGE concentration in each phase, we used laser ablation ICP-MS as a method of analysis. This technique measures the intensity of preselected isotopes as a function of ablation time, thus yielding a time-resolved depth profile for each analysis spot and hence allowing us to filter out the contribution of inclusions to the sample signal. To promote solution of Re and the PGE into all phases, experiments were done at Re and PGE concentrations in the sulfide melt up to metal saturation levels. To avoid Re volatilization, experiments were done at 1 GPa, using a piston-cylinder apparatus, and employed a growth protocol designed to promote the formation of a few, large chromite crystals, thus allowing for an expanded spot for laser ablation analysis and hence lower detection limits. A summary of partitioning experiments is provided in Table 1.

TABLE 1. Summary of Experiments

Experiment no.	Capsule[1]	Additives[2]	Soak (h)[3]	Total duration (h)	log f_{O_2}[4]	log f_{S_2}[5]	Alloys present[6]
IPRe4	A	1 wt % Ir, Pd and Re	48	73.5	–8.9(0.2)	–2.1(0.2)	$Ir_{57.2}Re_{38.1}Fe_{4.7}$
PGE1b	A	500 ppm PGE and Re	60	85.5	–9.5(0.2)	–2.1(0.3)	Quench
PGE1c	A	500 ppm PGE and Re	30	55.5	–9.2(0.3)	–1.6(0.2)	Quench
PGE1d	B	500 ppm PGE and Re	30	55.5	–9.2(0.2)	–1.8(0.2)	Quench
PGE1e	B	500 ppm PGE and Re	60	85.5	–9.3(0.3)	–2.0(0.2)	Quench

[1] Capsule configuration used in experiment: A = graphite-lined Pt, B = graphite-only Pt
[2] Approximate amount of each metal (Re + PGE) added to sulfide melt
[3] Duration of final soak step (1,330°C) following 1.5 h superliquidus (1,460°C), 4 h at the liquidus (1,350°C), and a 1°C/h ramp
[4] Calculated f_{O_2} based on the chromium content of silicate melt, using data in Roeder and Reynolds (1991)
[5] Calculated f_{S_2} using the calculated f_{O_2}, melt sulfur abundance and equation 7 of Wallace and Carmichael (1992)
[6] All experiments contained Re-PGE alloy as a quench phase in the sulfide liquid, experiment IPRe4 also contained an intergrowth of immiscible alloys, whose average composition is given in atomic percent

Experimental details

The silicate melt employed in our experiments corresponds to the 401 diabase composition of Hill and Roeder (1974), for which the chromite saturation surface as a function of temperature and oxygen fugacity has been extensively characterized (Hill and Roeder, 1974; Murck and Campbell, 1986; Roeder and Reynolds, 1991). This composition was synthesized from a mixture of high-purity oxides and carbonates that were ground under ethanol in an agate mortar, dried, decarbonated, and then preequilibrated at the magnetite-hematite buffer to ensure a high initial ferric/ferrous ratio. Following the decarbonation-oxidation steps, synthetic brucite was added to the starting material in an amount sufficient to release ~1 wt percent water at run conditions. Water was added because reconnaisance experiments showed that its presence appeared to enhance chromite growth, with only a few, relatively large (25–50 μm) chromites produced in wet runs, as opposed to numerous small crystals in those run nominally dry. The sulfide melt used in this study was prepared using a mixture of pure Fe, Ni, S powder in 50:20:30 ratio by weight, to which Re and PGE metals were added. The identity and approximate amount of each metal added to an experiment is provided in Table 1. Individual samples were prepared by combining ~10 mg of the 401 diabase composition with ~1 mg of the sulfide melt mixture using a clean razor blade, then loading into a graphite-lined Pt capsule and sealed using an arc welder. Experiments PGE1d and PGE1e were run in graphite only. Encapsulated samples were then inserted into a standard ¾" NaCl pyrex-crushable magnesia pressure cell and run at high P and T in the piston-cylinder apparatus. Each partitioning experiment consisted of four separate temperature steps: (1) an initial superliquidus step at 1,460°C, lasting 2 h to allow the silicate and sulfide melt mixture to homogenize; then (2) rapid cooling (50°C/min) to the predetermined liquidus (1,350°C) for 1.5 h to allow for nucleation of chromite crystals; followed by (3) slow cooling (1°C/h) to promote growth of chromite; and (4) an isothermal soak at 1,330°C of varying duration (20–60 h), then quenching.

Following an experiment, samples were initially sectioned by grinding with 400- and 600-grit paper, and upon exposing an appropriate amount of surface, mounted in epoxy resin media. After curing, mounted samples were then reground with 400- and 600-grit paper and polished with 1- and 0.3-μm alumina powder prior to textural observations and subsequent microbeam analysis.

Analytical Techniques

Major element analysis

Major element composition of run-product phases was obtained using a Cameca SX 50 electron microprobe at the University of Toronto. Glass analyses were carried out using a 15-μm defocused beam at 15-kV accelerating voltage, with two conditions: a 10-nA beam for major and minor elements and a 50-nA beam for Ni. Chromite grains were analyzed using an accelerating voltage of 20 kV and focused beam of 35 nA. Chemical homogeneity of chromite and glass phases in run products were determined by multiple analyses consisting of up to 10 points in chromite along the diagonal axes of the exposed crystals and 20 points in glasses along the horizontal and vertical length of the samples. Owing to their textural inhomogeneity, sulfide melt compositions were determined by combining focused beam analyses of quench phases (15-kV accelerating voltage, 25-nA beam current) with modal abundances determined by image analysis. Alloy compositions in the run product from experiment IPRe4 were determined using a 20-kV accelerating voltage and a focused beam current of 60 nA. Standards used for electron microprobe analysis were Juan de Fuca Ridge VG2 glass, natural chromite, pentlandite, and pure PGE and Re metals. Analyses of chromite- and sulfide-silicate melt are provided in Table 2.

Trace element analysis

We determined the trace element content of individual run-product phases using the laser ablation ICP-MS facility in the Department of Earth and Planetary Sciences at Harvard University. This system employs a Lambda Physik excimer laser (operating with an ArF mixture at 193 nm) coupled to a PQ II+ quadrupole ICP-MS, with He flushing the ablation cell to enhance sensitivity (Eggins et al., 1998). Further details of this system are provided in Horn et al. (2000). For calibration purposes, a silicate reference glass, NIST 610, doped with 61 trace elements at a level of approximately 450 and 49 ppm Re, and a Ni sulfide inhouse standard (PGE76) containing ~76 ppm of all PGE and trace levels of Re (~6 ppb) were selected. The standards were analyzed four times,

TABLE 2. Analyses of Chromite- and Sulfide-Silicate Melt

Sample	Phase	SiO_2	TiO_2	MnO	FeO	MgO	CaO	Al_2O_3	Cr_2O_3	Na_2O	S (ppm)	Total
a. Major and minor element composition (wt %) of glass and chromite												
IPRe4	Glass	52.31 (0.24)[1]	1.73 (0.19)	0.19 (0.05)	10.17 (0.14)	7.97 (0.10)	9.11 (0.16)	15.21 (0.11)	0.44 (0.03)	2.75 (0.11)	930 (150)	99.92
	Chromite	0.11 (0.01)	0.76 (0.01)	0.21 (0.01)	18.97 (0.12)	11.16 (0.16)		17.49 (0.23)	50.39 (0.29)			99.10
PGE1b	Glass	52.06 (0.35)	1.80 (0.18)	0.18 (0.05)	10.09 (0.18)	8.12 (0.12)	9.18 (0.10)	14.55 (0.10)	0.54 (0.04)	2.75 (0.12)	1430 (160)	99.91
	Chromite	0.16 (0.02)	0.75 (0.02)	0.22 (0.01)	18.77 (0.07)	10.97 (0.27)		14.85 (0.58)	53.97 (0.65)			99.67
PGE1c	Glass	51.88 (0.44)	1.92 (0.27)	0.18 (0.07)	9.82 (0.23)	8.04 (0.15)	9.38 (0.12)	14.25 (0.14)	0.49 (0.06)	2.57 (0.11)	1220 (210)	98.61
	Chromite	0.12 (0.07)	0.80 (0.04)	0.22 (0.01)	19.61 (0.13)	10.49 (0.29)		15.02 (0.88)	52.72 (0.21)			98.99
PGE1d	Glass	50.66 (0.73)	1.78 (0.21)	0.16 (0.05)	10.75 (0.38)	7.59 (0.11)	9.05 (0.12)	14.07 (0.12)	0.48 (0.04)	3.78 (0.12)	1320 (120)	98.63
	Chromite	0.12 (0.02)	0.77 (0.03)	0.21 (0.01)	20.16 (0.11)	10.24 (0.44)		14.34 (0.62)	53.67 (0.29)			99.52
PGE1e	Glass	51.51 (0.50)	1.77 (0.14)	0.15 (0.07)	9.50 (0.30)	7.82 (0.12)	9.16 (0.14)	14.41 (0.11)	0.50 (0.05)	2.85 (0.07)	1240 (140)	97.94
	Chromite	0.10 (0.01)	0.78 (0.03)	0.23 (0.01)	18.88 (0.08)	10.94 (0.25)		14.28 (0.36)	54.52 (0.39)			99.73

b. Major element composition (wt %) of sulfide liquids[2]

Experiment no.	Fe	Ni	S	Total
IPRe4	44.81 (1.60)	19.54 (1.80)	33.94 (0.30)	98.29
PGE1b	57.49 (1.34)	8.62 (1.51)	35.73 (0.25)	98.85
PGE1c	48.70 (0.97)	15.15 (1.09)	34.66 (0.18)	98.51
PGE1d	48.89 (2.07)	15.67 (1.21)	34.39 (1.02)	98.95
PGE1e	47.18 (3.14)	16.87 (3.54)	34.38 (0.58)	98.42

[1] Number in parentheses is 1σ of 20 glass analyses or 10 chromite analyses

[2] Melt composition determined by combining individual quench phase compositions (5 or more analyses of each) with their modal abundances, quoted uncertainty is based on the combined error in modal abundance estimates and the variation in quench phase analyses

twice before and after analysis of 16 points on each sample. Each spot analysis consisted of 60 s of background measurement (gas blank) followed by ~60 s of sample ablation. The intensity for each element was calculated as the mean count rate during the ablation period corrected for differences in the ablation yield using a known internal standard element. ^{55}Mn, ^{49}Ti, and ^{43}Ca were used as internal standards to correct for ablation yield differences, since their concentrations in the glass, chromite, and the NIST 610 standard are known. ^{61}Ni was used as an internal standard to monitor the PGE concentrations using the PGE76 NiS standard. In all run products the Ni content of the chromite and silicate melt were lower than the detection limit of the electron probe, thus, Ni concentrations in these phases were measured by LA-ICP-MS using the NIST 610 glass as standard. These values were then used to correct for ablation yield differences and to calculate PGE concentrations using the PGE76 standard. In this study, isotopes measured in glass, chromite and sulfide consist of the following: ^{61}Ni, ^{62}Ni ^{99}Ru, ^{101}Ru, ^{102} Ru, ^{103}Rh, ^{105}Pd, ^{185}Re, ^{190}Os, ^{192}Os, ^{191}Ir, ^{193}Ir, and ^{195}Pt. By using the time-resolved spectra, it was possible to observe the presence of any heterogeneity as expressed by intensity variations during the actual analysis. The most common heterogeneity encountered was high concentration spikes in PGE concentrations corresponding to microinclusions within various phases. Therefore, in order to determine PGE contents of inclusion-free material, each spectrum was examined individually and only spike-free domains were integrated to calculate the trace element concentrations. The precision and detection limits of the LAM-ICP-MS are discussed in detail in Jackson et al. (1992) and Jenner et al. (1993). The minimum detection limit is determined by count rates that are 2σ above background. It is important to point out that this detection limit is not constant and varies with the ablation efficiency and the pit size. The ablation yield is a measure of how a particular phase ablates in comparison to the NIST 610 glass or PGE 76 standard. Thus, minimum detection limits are generally lower in glass and sulfide since large ablation craters were produced during those measurements (85–180 μm). In contrast, the minimum detection limits in chromites were high owing to the small ablation spots, which ranged from 15 to 20 μm.

In the case of quenched sulfide melt, the extreme textural inhomogeneity of this material prevented us from accurately determining trace element contents by in situ methods. The Re and PGE contents of sulfide melts from experiments PGE1b-e were estimated by mass balance, using whole-sample concentrations determined by instrumental neutron activation analysis (INAA). Experiment IPRe4 was saturated in Ir-Re alloy, so Re and PGE abundances in the sulfide liquid could not be determined by this method. Subsequent to the in situ analyses, sectioned samples were extracted from their mounts using a diamond wafering blade, cleaned of adhering graphite, then irradiated along with standards for 30 h at the SLOWPOKE II reactor facility at the Royal Military College (Ontario, Canada). Samples and standards were then counted using a thick planar-type intrinsic Ge detector at the University of Toronto. Chromium and gold are present in our samples at the wt percent and parts per million levels, respectively, with the latter element being a contaminant in the reagents used as starting materials. Owing to large interferences produced by the decay of Cr and Au isotopes, abundances of Rh and Pt could not be determined by INAA. Although logistical difficulties prevented us from counting the 88.04 keV gamma ray associated with short-lived ^{109}Pd at the reactor site, Pd abundances were determined using the 21.90 keV X-ray, for which we have greater detector sensitivity. Despite this measure, overall low count rates from ^{109}Pd decay resulted in poor precision in determining the abundance of this element. Whole-sample Ni abundances measured by INAA, combined with values determined in situ for sulfide and silicate melts, were used to estimate the mass fraction of these two phases present within the aliquot of run product analyzed by INAA. Inasmuch as the Re and PGE content of silicate glass is essentially zero, abundances of these elements in the sulfide melt could be estimated by dividing whole-sample concentrations by the mass fraction of sulfide melt. A complete summary of whole sample, sulfide melt, and in situ trace element determinations is provided in Table 3.

Results and Discussion

Textural observations

Figure 1A shows a portion of a sectioned run product and provides an example of the typical textural development in our experiments. Silicate melts are quenched to glass and lack visible quench crystals, except at the margins of some chromite grains. Chromites are generally sub- to euhedral, vary in size from 20 to 50 μm, and ares nucleated either on the walls of the graphite capsule or at the sulfide and/or silicate liquid interface. Chromite crystals frequently contain inclusions of sulfide melt (Fig. 1B), which were entrapped during nucleation and growth. Quenched sulfide liquid occurs as circular globules, ranging from 80 to 450 μm in diameter, and commonly adheres to the wall of the graphite capsule (Fig. 1A, D) and to chromite crystals. Sulfide globules are texturally inhomogeneous (Fig. 1C, D), which is presumably a result of rapid crystallization during the quench. Re-PGE alloy occurs as an interstitial quench phase (Fig. 1C) within the sulfide globules of all experiments. Experiment IPRe4, which contained the highest abundance of added Re and PGE (1 wt % each of Ir and Re), also produced relatively large (>10 μm) euhedral crystals of Ir-Re alloy, hosting fine, bladed crystals of a second, presumably immiscible Ir-Re alloy. Both alloys are interpreted to have been stable during the experiment. Because of the finely intergrown texture in these alloys, we could not obtain reliable analyses for each, although they were confirmed as compositionally distinct by qualitative energy dispersive analysis. As such, the alloy composition provided in Table 1 is probably an average, whereas estimates of each phase composition can be made using the Ir-Re phase diagram (see "PGE mass balance in chromitites" section). These alloy intergrowths only occur within sulfide globules, which probably reflects the preferential wetability of the sulfide melt for the metallic phase, as also observed by Brenan and Andrews (2001).

Major and minor element behavior

Electron microprobe analyses across individual chromite phenocrysts reveal them to be homogeneous, as the standard

TABLE 3. Summary of PGE, Re, and Ni Concentrations (ppm) in Run Product Phases

Sample no.	Phase	n[1]	Ni	Ru	Rh	Pd	Re	Os	Ir	Pt
IPRe4	Glass	9	240 (46)	<0.05[2]	<0.020	<0.12	0.041 (0.016)	<0.038	<0.040	<0.45
	Chromite	1	850	<2.5	<0.13	<0.087	<0.06	<0.61	<0.15	<1.0
	Sulfide		see Table 2b	NR[3]	NR	NR	NR	NR	NR	NR
PGE1b	Glass	4	90 (9)	<0.030	<0.010	<0.050	0.016 (0.003)	<0.020	<0.010	<0.030
	Chromite	2	610 (43)	<1.5	<0.80	<3.6	<0.38	<0.97	<0.35	<1.2
	Sulfide[4]		see Table 2b	1035 (56)	ND[5]	459 (91)	542 (1)	1937 (11)	352 (1))	ND
PGE1c	Glass	5	160 (57)	<0.053	<0.040	<0.16	0.016 (0.006)	<0.019	<0.02	<0.057
	Chromite	1	890	<1.4	<0.33	<0.18	<0.59	<0.18	<0.15	<0.91
	Sulfide		see Table 2b	1120 (32)	ND	659 (152)	837 (1)	1627 (6)	714 (1)	ND
PGE1d	Glass	3	120 (5)	<0.057	<0.020	<0.10	0.013 (0.005)	<0.026	<0.020	<0.031
	Chromite	1	732	<1.20	<0.89	<2.5	<0.53	<1.40	<0.37	<1.4
	Sulfide		see Table 2b	694 (37)	ND	441 (80)	628 (1)	782 (6)	515 (1)	ND
PGE1e	Glass	4	140 (11)	<0.075	<0.010	<0.060	0.012 (0.002)	<0.010	<0.01	<0.020
	Chromite	2	590 (68)	<0.52	<0.52	<2.6	<0.36	<0.51	<0.14	<0.61
	Sulfide		see Table 2b	604 (35)	ND	465 (105)	387 (1)	619 (6)	487 (1)	ND

[1] Refers to number of analyses used to obtain average
[2] Concentrations given as less than detection (defined as 2σ above background) correspond to lowest measured values amongst multiple analyses
[3] No value reported due to sample heterogeneity during LA-ICPMS analysis and because alloy saturation prevented determination by mass balance
[4] Sulfide melt Re and PGE concentrations determined by mass balance using whole-sample PGE abundances measured by INAA (see text)
[5] Element abundance not determined due to high concentration of interfering element (Cr on Rh and Au on Pt; see text)

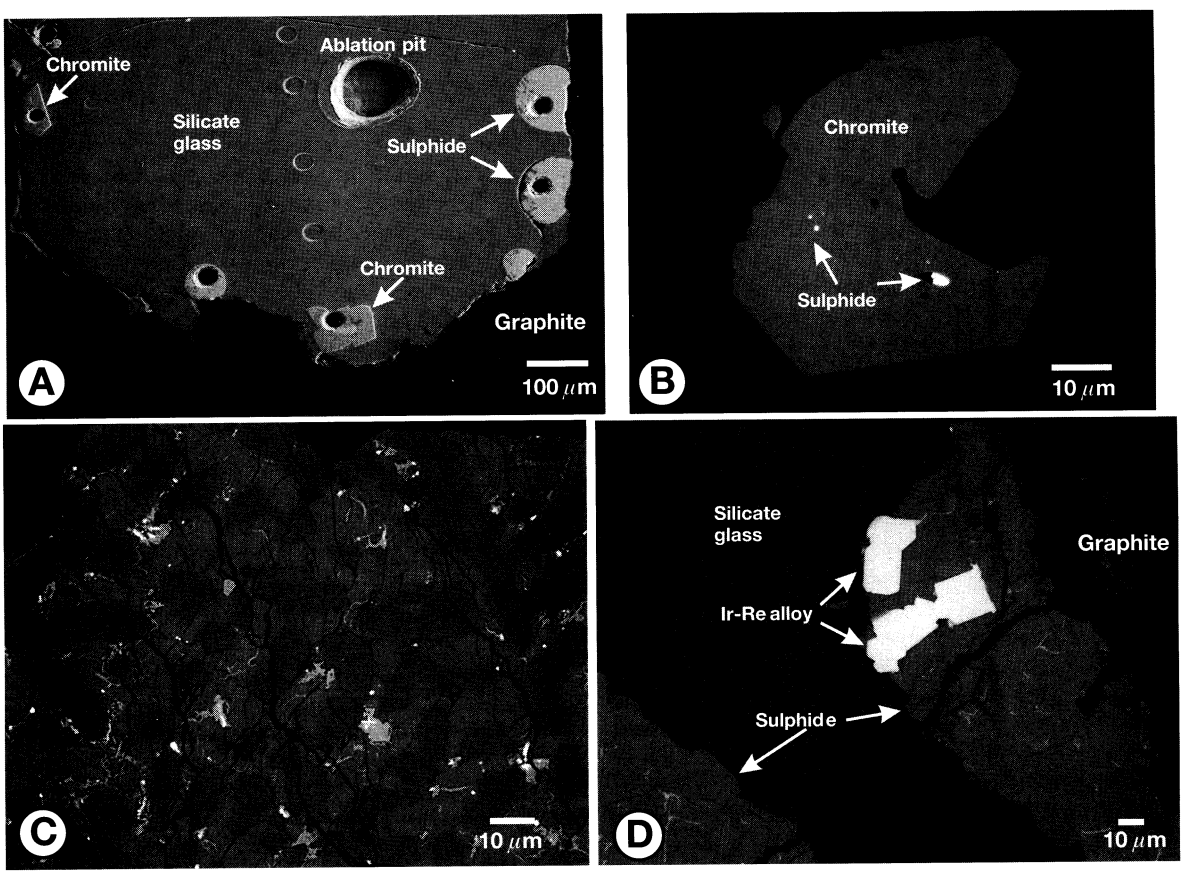

FIG. 1. A. Secondary electron image of a sectioned run product, showing the typical textural association of phases produced in partitioning experiments. The circular structures correspond to the ablation pit (as labeled in silicate glass) produced during trace element analysis. B. Backscattered electron image of a chromite crystal produced in experiment PGE1b. Note the inclusions of sulfide liquid trapped during crystal growth. Using time-resolved analysis, the trace element contribution from these inclusions can be excluded, yielding the intrinsic abundance in the chromite. C. Backscattered electron image of quenched sulfide melt from experiment PGE1d. The image reveals domains of variable metal content produced during the quenching process. High Fe, low Ni domains are dark in this image, with brightness increasing with Ni content. The low abundance, brightest regions contain the highest concentrations of PGE. D. As in C, from experiment IPRe4. In addition to containing the PGE-rich domains produced during the quenching process, this sample was also saturated in discrete crystals of Ir-Re-rich alloy (as shown), interpreted to have been a stable phase during the experiment.

deviation in analyses is generally similar to errors from counting statistics. Figure 2 compares the trivalent cation compositions (calculated assuming AB_2O_4 stoichiometry) of naturally occurring chromites to those produced in this study. Our synthetic chromites fall within the range of compositions from ophiolites, alpine peridotites, and layered intrusions, which are all characterized by low aluminum and ferric iron contents. Glass analyses from analytical traverses both across and down the length of a run product reveal the same level homogeneity. Such results are also confirmed by the reproducibility of the minor and trace element (Ti, Mn, Ni) content of chromites and glasses measured by LA-ICP-MS. Although sulfide melt compositions are relatively imprecise, Fe, Ni, and S abundances are similar to amounts added initially. The notable exception to this is the melt from experiment PGE1b, which has an unusually low Ni abundance (~9 wt %) relative to initial values (~20 wt %). It is not clear why the Ni abundance is so different from the starting material, although possibilities include preferential Ni loss to the Pt capsule or simply variation in the Fe/Ni ratio in the added sulfide melt mixture, as a consequence of nugget effects. It seems most likely, however, that Ni loss by diking through the graphite capsule would also have reduced Fe abundances in the silicate melt, which is not observed. We therefore view the latter scenario as more likely, as it also probably accounts for the small but systematic differences between the initial sulfide mixture and the final melt composition seen in the other experiments.

Estimation of oxygen and sulfur fugacity

The prevailing oxygen fugacity within our experiments was estimated from the chromium content of the silicate melt, as

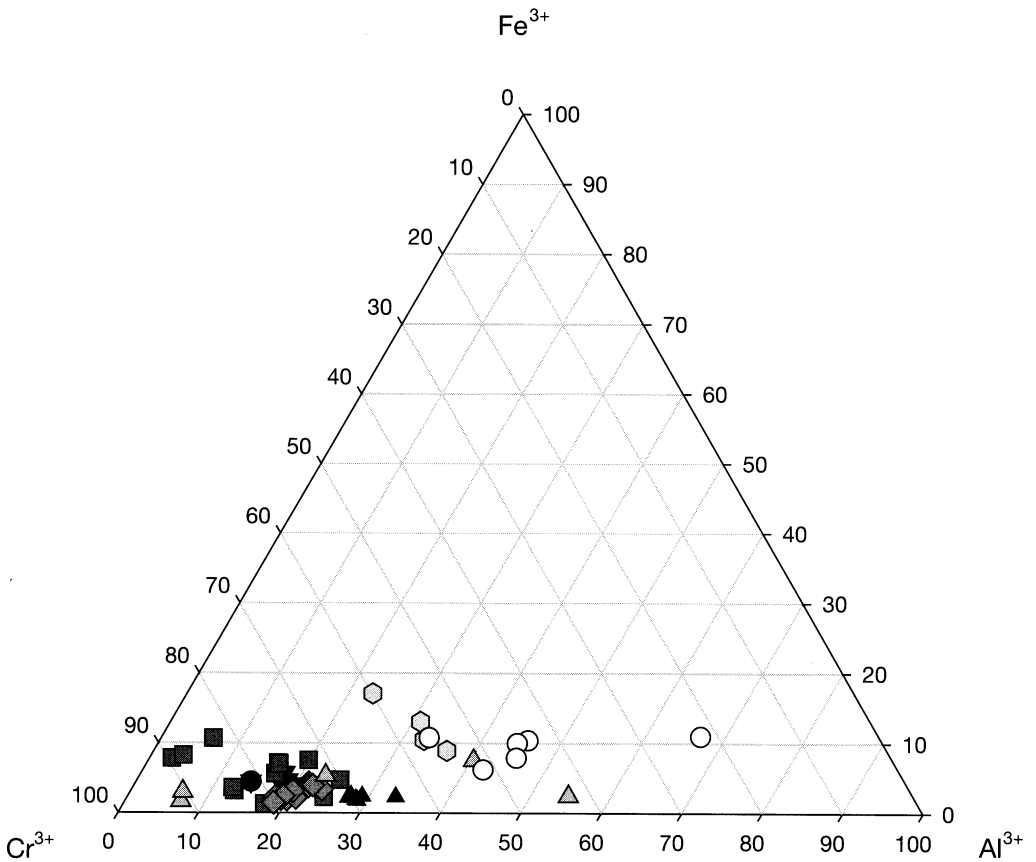

● **Oregon** - Alpine chromitites (Stockman and Hlava, 1984)
▼ **China** - Podiform chromitites (Zhou et al., 1996)
■ **Bulgaria** - Eastern Rhodhope Complex (Tarkian et al., 1991)
◆ **Greece** - Vourinos Ophiolite Complex (Roberts, 1982)
△ **Tasmania** - Heazlewood River Complex (Peck and Keays, 1990)
⬡ **South Africa** - Bushveld Complex (McLaren and De Villiers, 1982)
○ **Iceland** - Alkali basalt spinels (Thy, 1983)
▲ **This Study**

FIG. 2. Ternary plot depicting the chromite compositions (trivalent cation %) synthesized in this study in comparison to naturally occurring samples from different geologic settings.

deviation in analyses is generally similar to errors from counting statistics. Figure 2 compares the trivalent cation compositions (calculated assuming AB_2O_4 stoichiometry) of naturally occurring chromites to those produced in this study. Our synthetic chromites fall within the range of compositions from ophiolites, alpine peridotites, and layered intrusions, which are all characterized by low aluminum and ferric iron contents. Glass analyses from analytical traverses both across and down the length of a run product reveal the same level homogeneity. Such results are also confirmed by the reproducibility of the minor and trace element (Ti, Mn, Ni) content of chromites and glasses measured by LA-ICP-MS. Although sulfide melt compositions are relatively imprecise, Fe, Ni, and S abundances are similar to amounts added initially. The notable exception to this is the melt from experiment PGE1b, which has an unusually low Ni abundance (~9 wt %) relative to initial values (~20 wt %). It is not clear why the Ni abundance is so different from the starting material, although possibilities include preferential Ni loss to the Pt capsule or simply variation in the Fe/Ni ratio in the added sulfide melt mixture, as a consequence of nugget effects. It seems most likely, however, that Ni loss by diking through the graphite capsule would also have reduced Fe abundances in the silicate melt, which is not observed. We therefore view the latter scenario as more likely, as it also probably accounts for the small but systematic differences between the initial sulfide mixture and the final melt composition seen in the other experiments.

Estimation of oxygen and sulfur fugacity

The prevailing oxygen fugacity within our experiments was estimated from the chromium content of the silicate melt, as

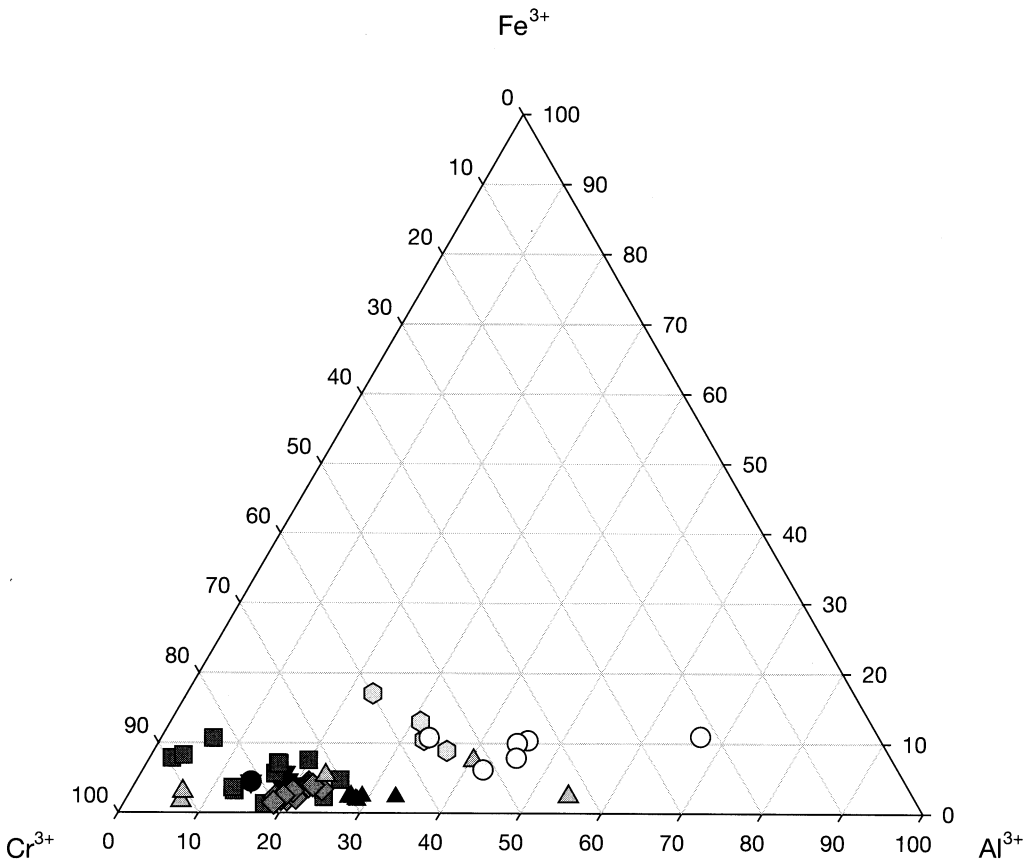

● **Oregon** - Alpine chromitites (Stockman and Hlava, 1984)
▼ **China** - Podiform chromitites (Zhou et al., 1996)
■ **Bulgaria** - Eastern Rhodhope Complex (Tarkian et al., 1991)
◆ **Greece** - Vourinos Ophiolite Complex (Roberts, 1982)
△ **Tasmania** - Heazlewood River Complex (Peck and Keays, 1990)
⬡ **South Africa** - Bushveld Complex (McLaren and De Villiers, 1982)
○ **Iceland** - Alkali basalt spinels (Thy, 1983)
▲ **This Study**

FIG. 2. Ternary plot depicting the chromite compositions (trivalent cation %) synthesized in this study in comparison to naturally occurring samples from different geologic settings.

this quantity is sensitive to f_{O_2} when the system is saturated in chromite (Murck and Campbell, 1986; Roeder and Reynolds, 1991). In this estimation, we parameterized the 1-bar experimental data of Roeder and Reynolds (1991) to obtain a polynomial expression for the Cr content of chromite-saturated 401 diabase as a function of f_{O_2} and temperature. Roeder and Reynolds (1991) also found that chromite solubility increased with pressure, and this effect was accounted for by shifting f_{O_2} calculated from the 1-bar parameterization by 0.68 log units. With this estimate of f_{O_2} combined with measured melt sulfur contents, sulfur fugacity (f_{S_2}) was calculated using the relationship derived by Wallace and Carmichael (1992; their eq 7). Values of f_{O_2} and f_{S_2} are provided in Table 1 and pertain to the final soak temperature of 1,330°C. Quoted uncertainties in f_{O_2} were determined by propagating the 1σ error in melt Cr content through the polynomial expression. Uncertainty in f_{S_2} is based on propagating the error in f_{O_2} through equation 7 of Wallace and Carmichael (1992). Taking these uncertainties into account, the between-run reproducibility of f_{O_2} and f_{S_2} is very good, and average log values are –9.2, and –1.9, respectively. For reference, calculated values of f_{O_2} correspond to 2.2 log units more reduced than the fayalite-magnetite-quartz (FMQ) buffer and values of f_{O_2} and f_{S_2} are within the range recorded by terrestrial oceanic basalts (Wallace and Carmichael, 1992). As experiments were contained in graphite and had initially high Fe^{3+}/Fe^{2+}, f_{O_2} is expected to decrease (approaching the CCO buffer) as a consequence of Fe reduction coupled to graphite oxidation (e.g., Holloway et al., 1992). At 1.0 GPa and 1,330°C, the CCO buffer is at a log f_{O_2} of –8.2 (Ulmer and Luth, 1991), and thus our experiments are behaving as expected, although f_{O_2} values are systematically more reduced than CCO, which is a consequence of adding sulfur to the system (see discussion in Peach and Mathez, 1993).

Trace Element Behavior

Distribution within individual phases

Analysis of chromites for trace elements was made difficult by the relatively small size of this phase in run products (20–50 μm) and its tendency to include other phases. As such, time-integrated signals were often short, as the laser quickly ablated through such small grains, and signals were often dominated by inclusion material. An example of this latter effect is shown in Figure 3A, which depicts the time-resolved ICP-MS spectra for a chromite grain from experiment IPRe4. As illustrated using the Pt and Ir signals, it is clear that this grain contains PGE-rich domains, interpreted as included sulfide globules, as confirmed by high resolution imaging (Fig. 1B). Using time-resolved analysis, however, we are able to avoid these domains and thus provide the most accurate measure of the intrinsic Ni, Re, and PGE content of each chromite grain. In all cases, these best estimates of chromite Re and PGE contents yielded values that were below detection. In contrast, clean chromite domains yielded uniform and measurable Ni concentrations.

There was substantial variation in the signal intensity during laser ablation of the quenched sulfide globules, and an example of this behavior is portrayed in Figure 3B. This variation arises from the sequential ablation of different quench phases and clearly precludes the accurate determination of element concentrations in the prequench sulfide liquid. In addition to the intraspot heterogeneity, we also encountered significant spot to spot variability in the average signal intensity for a particular element, which we attribute to differences in the depth over which the average was taken (i.e., some globules were thinner than others, reflecting significant phase loss during polishing) and the overall coarseness of the quench crystals. As such, sulfide melt Re and PGE concentrations reported in Table 3 correspond to values measured by whole-sample INAA. No sulfide melt analyses are reported for experiment IPRe4, as this experiment was alloy saturated, thus precluding the mass-balance approach based on whole-sample abundances.

Silicate glasses contain relatively high and uniform concentrations of Ni and Re, whereas the PGE exhibit variable behavior, depending on whether the experiment was alloy saturated or not. For the case of experiment IPRe4, which contained clearly visible phenocrysts of Ir-Re alloy, all of the PGE exhibited a heterogeneous distribution in the silicate melt (Fig. 3C). In contrast, PGE-rich, but stable alloy-free experiments had glass PGE contents that were below minimum detection limit (Fig. 3D), with only occasional PGE-rich spikes (i.e., contamination zones). In the former experiments, the PGE-rich domains observed in the time-resolved spectra probably arise from the intersection of PGE micronuggets, as has been proposed in previous work involving alloy-saturated systems (e.g., O'Neill et al., 1995; Ertel et al., 1999). In the latter experiments, the occasional PGE-rich spikes are probably derived from discrete sulfide microglobules. Aside from these occasional spikes, the lack of associated PGE in glass analyses from alloy-undersaturated experiments suggests that the Re signal from the glass is not derived from dispersed sulfide microglobules but instead from a dissolved component of the silicate melt. The solubility of pure Re at the f_{O_2} of our experiments is estimated to be ~0.013 ppm, based on the measurements of Ertel et al, (2001) from experiments done at 1 bar involving an iron- and sulfur-free melt composition. The Re contents of the glasses produced in our alloy-undersaturated experiments are similar to this value (0.012–0.016; Table 3), whereas the Re content of glass from the Ir-Re alloy-saturated experiment (IPRe4) is higher (0.041 ppm). At conditions close to saturation, a small amount of stable alloy might be overlooked, given the extremely low solubility of rhenium. However, it is important to point out that in the presence of other siderophile elements, any saturating alloy will contain some amount of these other elements, and thus enhanced levels of Re in the melt due to the presence of dispersed micronuggets would also be associated with enhanced levels of other PGE, which is not observed. Moreover, although O'Neill et al (1995) argued that S should not affect the solubility of siderophile elements in silicate melt, Amossé et al. (2000) have shown that Rh, Ir, and Pt solubility markedly increase with increasing f_{S_2}. Also, Peach et al. (1994) obtained silicate melts with up to 300 ppb Ir in alloy-undersaturated, sulfide-silicate melt partitioning experiments, a level that far exceeds the value of ~30 ppb for the solubility of Ir in the sulfur-free experiments of O'Neill et al. (1995). Thus, the lack of evidence for stable Re-bearing alloy in what we interpret as alloy-undersaturated experiments is most likely to be

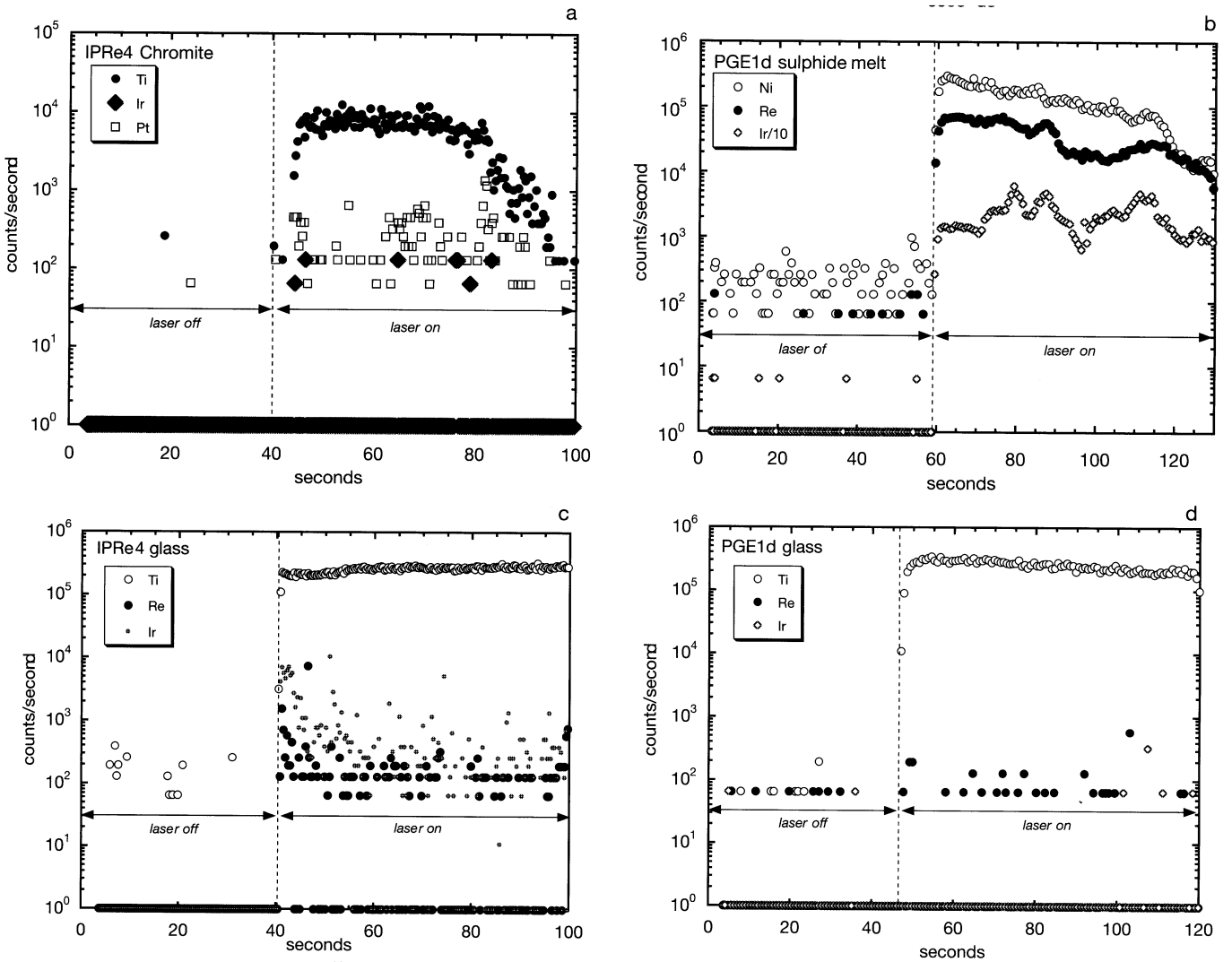

FIG. 3. Time-resolved spectra produced during laser ablation of various run-product phases. A. Chromite from experiment IPRe4. Note the heterogeneous distribution of Pt, which is interpreted as derived from inclusion material, and the correlation between Ir and Pt concentrations. B. Sulfide melt from experiment PGE1d. The variation in Ni, Re, and Ir contents with time (= depth) reflects the textural inhomogeneity of the quenched melt. C. and D. Glasses from experiments IPRe4 (alloy saturated) and PGE1d (alloy undersaturated), respectively. Note that Re is relatively homogeneous in each of these glasses, whereas Ir is highly inhomogeneous in the alloy-saturated glass, suggesting that Ir-bearing micronuggets are sampled during analysis. Ir micronuggets appear to be absent in the alloy-undersaturated glass.

a consequence of enhanced Re solubility due to the presence of dissolved sulfur.

Trace element partitioning

Sulfide melt-chromite, chromite-silicate melt, and sulfide-silicate melt partition coefficients (D) for Ni, Re, and PGE are summarized in Table 4. Chromite- and sulfide-silicate melt partitioning of nickel and rhenium allows us to make a first-order assessment of the approach to phase equilibrium in our experiments. In addition to the general homogeneity of Ni in chromite and silicate melt, Ni partitioning between these phases is reproducible between experiments, with values ranging from ~4 to ~7, with no systematic variation with run duration or encapsulation technique (Fig. 4). Our partition coefficients for Ni are similar to those determined for Co (i.e., 5 ± 0.5) by Horn et al. (1994) involving chromium-rich spinel, which is not unexpected, given the similar charge and ionic radius of these elements. Sulfide-silicate melt partition coefficients for Re and Ni are similarly reproducible (Fig. 4), despite the imprecision in the sulfide melt Ni determinations. Partition coefficients for Ni (810–1,300) are in good accord with the values of 1031 to 1422 determined by Peach and Mathez (1993) at similar conditions of P, T, f_{O_2}, and melt FeO content. In terms of the approach to sulfide-silicate melt equilibrium for the PGE, Bezmen et al. (1994) showed that partition coefficients for these elements become constant at run durations as short as 30 h, suggesting that the approach to two-liquid equilibrium is rapid. All of our experiments were run for at least 30 h, indicating that the minimum partition coefficients determined in this study are most likely to represent equilibrium values.

TABLE 4. Summary of Partition Coefficients between Sulfide and Silicate Melt or Chromite

Experiment no.	Phase	Ni	Ru	Rh	Pd	Re	Os	Ir	Pt
IPRe4	Sulfide/silicate	810 (170)							
	Sulfide/chromite	230 (21)							
	Chromite/silicate	3.5 (0.7)				<1.5			
PGE1b	Sulfide/silicate	960 (190)	>35000		>9180	34000 (6400)	>97000	>35000	
	Sulfide/chromite	140 (26)	>690		>130	>370	>2000	>1000	
	Chromite/silicate	6.8 (0.8)				<24			
PGE1c	Sulfide/silicate	950 (350)	>21000		>4119	52000 (20000)	>86000	>36000	
	Sulfide/chromite	170 (12)	>800		>3700	>85	>1800	>4800	
	Chromite/silicate	5.6 (2.0)				<37			
PGE1d	Sulfide/silicate	1300 (110)	>12000		>4110	48000 (19000)	>30000	>26000	
	Sulfide/chromite	214 (17)	>580		>180	>430	>560	>1400	
	Chromite/silicate	6.1 (0.3)				<41			
PGE1e	Sulfide/silicate	1200 (270)	>8100		>7750	33000 (5400)	>62000	>49000	
	Sulfide/chromite	290 (69)	>1200		>180	>610	>1200	>3500	
	Chromite/silicate	4.2 (0.6)				<30			

Minimum sulfide-silicate melt partition coefficients for the PGE from a particular experiment were calculated using the PGE content of the sulfide melt combined with the maximum PGE content of the silicate melt, based on the silicate melt analysis with the lowest minimum detection limit. The highest minimum values determined in this study, along with measured Re partition coefficents, are compared to previous determinations in Figure 5. Our highest minimum estimates for PGE partition coefficients are 0.4 to10 ? 10^4 and are similar to values determined in previous studies. As can be seen in Figure 5, substantial variation exists in the dataset for sulfide-silicate melt partitioning of the PGE. The origin of this variation has been debated for some time, and there is still disagreement as to the role of f_{O_2}, T, melt composition, and PGE concentration in producing this behavior (cf. Bezmen et al., 1994; Fleet et al., 1996). A common aspect of all previous determinations, however, is the use of bulk analytical techniques to determine the PGE content of mechanically separated run products. Inasmuch as PGE-rich spikes were observed in our time-resolved glass analyses, we suggest that part of the variability of previous determinations may also arise from incomplete phase separation, as even small amounts of sulfide included in the glass phase would lower partition coefficients. Indeed, although Fleet et al. (1996) were able to acquire reproducible analyses on various-sized glass fractions from their run products, the scale of heterogeneity we observe is on the scale of microns or less. Our data further affirm the extreme nature of sulfide-silicate melt partitioning of the PGE and clearly reinforce the essential conclusion of previous experimental studies: segregation of even small amounts of magmatic sulfide liquid will strongly concentrate all of the PGE and profoundly influence the behavior of these elements during melting and solidification.

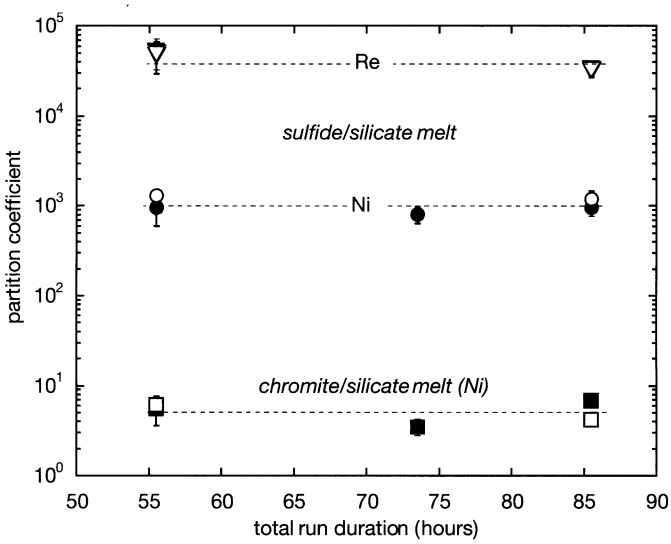

FIG. 4. Variation in sulfide-silicate melt (Re, Ni) and chromite-silicate melt (Ni) partition coefficients as a function of experiment duration. Data are shown for samples sealed in graphite-lined (filled symbols) and graphite-only (open symbols) platinum capsules.

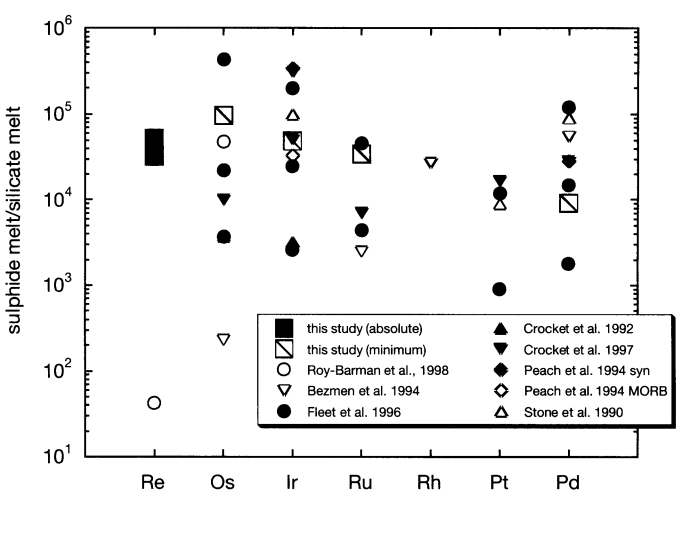

FIG. 5. Comparison of sulfide-silicate melt partition coefficients measured in this study with values reported in the literature (sources as shown). The partition coefficients for Re constitute the range of values determined in this study, whereas values for the PGE correspond to the highest minimum value measured among all experiments (see Table 4).

Our sulfide-silicate melt partition coefficients for Re are 3.3 to 5.2 × 10^4 and substantially greater than the partition coefficient of 43 determined by Roy-Barman et al. (1998) involving bulk analyses of glass and sulfide phases separated from a Loihi seamount lava. Given that their estimate of the sulfide-silicate D for osmium (4.8 × 10^4) is consistent with the minimum value we have measured, the substantial discrepancy in the value for Re is somewhat puzzling. In either case, results suggest that Re is sequestered by the sulfide liquid, although our data indicate that the efficiency of collection will be much greater. It is also of note that all of our sulfide-silicate melt D values for Re are less than our highest minimum estimate for Os (9.7 × 10^4), implying that sulfide liquid, either as a mantle residue or removed at low pressure, can fractionate Re from Os (by at least a factor of 3), thus contributing to the observed Os depletion in mantle-derived magmas.

As a consequence of the exceedingly low solubility of the PGE in molten silicate, we were not able to obtain bounds on the chromite-silicate melt partitioning behavior of these elements. However, for the case of Re, results from experiment IPRe4 yielded the lowest minimum detection limits for this element in chromite, thus providing a best estimate maximum partition coefficient of 1.5. In contrast to the relatively low D_{Re} inferred for chromite, Righter et al. (1998) have shown that Re is highly compatible in magnetite, with D_{Re} ranging from 20 to 50. The maximimum D_{Re} we have measured for chromite is also lower than the value of ~3 measured for garnet-silicate melt by Righter and Hauri (1998). These results would suggest that the behavior of Re in igneous systems will not only be influenced by the presence of sulfide melt but also by the identity of the crystallizing oxide phase and whether melting occurs in the spinel or garnet facies.

PGE mass balance in chromitites

Constraints on chromite-sulfide melt partitioning allow for a direct assessment of the relative roles of these phases in PGE collection in sulfide-saturated systems. Minimum sulfide melt-chromite partition coefficients were calculated using the minimum detection limits for these elements in chromite, combined with concentrations in coexisting sulfide melt. The highest minimum partition coefficients calculated in this way exceed 1,000, clearly indicating that coexisting sulfide melt will be the dominant host for the PGE. The spinel- and magnetite-silicate melt partition coefficients for Ru and Rh determined at much higher f_{O_2} by Capobianco et al. (1994) vary from ~2 to ~200× less than typical sulfide-silicate melt values of ~10^4. Our direct determinations of sulfide melt -chromite partitioning clearly indicate that the disparity in PGE partitioning will be much greater than this, however, which is probably a consequence of changes in the spinel structure by Cr substitution, and the concomitant shift in ionic radius that accompanies the change in oxidation state of the PGE with reduction in f_{O_2}.

Using the sulfide melt-chromite partitioning data, we calculated a mass balance for the system to assess the maximum likely contribution from chromite to whole-rock PGE abundances in sulfide-saturated samples. Assuming sulfide melt-chromite equilibrium, we have calculated the mass balance for Ir in chromitites from the Bushveld, using the whole-rock Ir and sulfur concentrations summarized in Maier and Barnes (1999). Ir was chosen in this example as it is an IPGE that frequently occurs in high abundance in chromitities and is best constrained in terms of lower bounds in sulfide-chromite fractionation. In this example, sulfide melt fractions were calculated from whole-rock sulfur contents by assuming 30 wt percent sulfur in the sulfide melt phase. The maximum iridium content of chromite, and hence the minimum iridium content of coexisting sulfide melt, was calculated using a minimum sulfide melt-chromite D_{Ir} of 4.8 × 10^3 (experiment PGE1c, Table 4). Figure 6A illustrates the calculated variation in the (maximum) percent Ir in chromite with the whole-rock sulfur content, along with the position of three chromitite reefs with measurable sulfur contents. For rocks with greater than 100 ppm sulfur, less than 38 percent of the Ir will be in chromite, and this value drops to less than 24 percent for rocks with >200 ppm sulfur. This example clearly illustrates that even for rocks with very low sulfur contents, chromite is not the significant PGE host.

An additional constraint on whether chromite serves as a significant PGE host in natural chomitites can be derived from the results of experiment IPRe4, which was saturated in Ir-Re alloy. In this experiment, we measured a maximum iridium concentration in run-product chromites of 150 ppb, which, when combined with an estimate of the Ir activity in the coexisting alloy, can be used to place upper bounds on the iridium solubility in chromite. With this information, it can be determined if the Ir content of natural chromitites exceeds this solubility level, thus indicating the importance of other PGE-bearing phases to the whole-rock PGE budget. The average composition of the alloy intergrowth in experiment IPRe4 was determined to be $Ir_{57}Re_{38}Fe_5$ (atomic %), which when projected onto the binary Ir-Re phase diagram (Okamoto, 1992) plots within the two-alloy field (Ir-rich side), confirming the textural observations and indicating that it is a two-phase intergrowth of $Ir_{70}Re_{30}$ and $Ir_{40}Re_{60}$ (the partitioning of Fe between alloys being unknown, but the small amount of Fe present is assumed to have a negligible effect on phase compositions). Accurate estimation of the activity of Ir in the alloy is made difficult by the lack of activity-composition data for the binary system. However, recognizing that immiscibilty in this system reflects a positive deviation from Raoult's law (e.g., Darken and Gurry, 1953), the activity coefficient for Ir in the alloy will be >1. Consequently, the maximum iridium solubility in chromite is expected to be ~210 ppb, based on the inferred presence of $Ir_{70}Re_{30}$ alloy and using a minimum activity coefficient of 1. A histogram depicting the Ir content of chromitites from various geologic settings is provided in Figure 6B and shows a preponderance of values <210 ppb but several samples having concentrations that exceed this value. Our results would suggest that the latter samples have Ir contents that could not be accommodated in chromite alone and strongly indicates that these chromitites have accumulated an additional PGE-bearing phase, such as trapped sulfide melt or accessory laurite and/or Ir-rich alloy. It is notable that these latter accessory phases are well documented in samples from all of the localities portrayed in Figure 6B. In agreement with this analysis are the results of Schoenberg et al. (1999) who have clearly demonstrated that

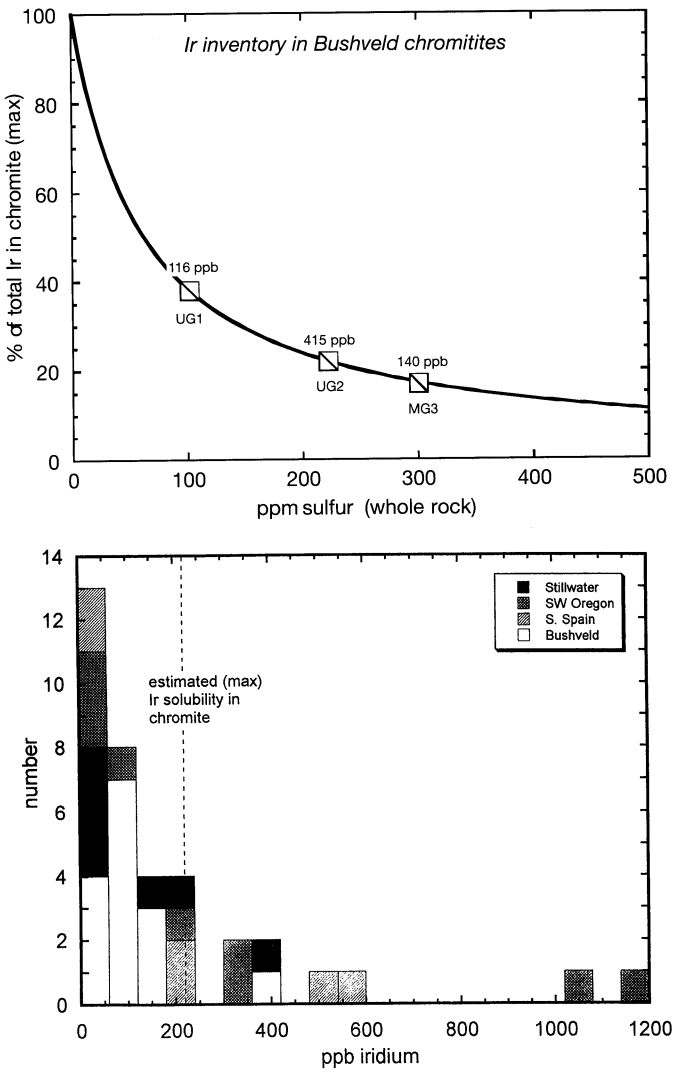

FIG. 6. A. Calculated iridium inventory (chromite vs. sulfide) as a function of whole-rock sulfur content for chromite in equilibirum with various sulfide fractions. In this case, the percent of Ir in chromite is calculated from mass balance, using a minimum sulfide/chromite partition coefficient of 4800 (Table 4) and assuming that sulfide melt contains 30 wt percent sulfur. For comparison are the sulfur contents of chromitites from the Bushveld Complex (summarized in Maier and Barnes, 1999). Each sample is labeled with its whole-rock Ir concentration. B. Histogram depicting the whole-rock Ir contents of chromitites from various geologic settings. The vertical dashed line corresponds to the maximum estimated solubility of Ir in chromite based on results from this study (see text for discussion). Data sources are Stockman and Hlava (1984), Talkington and Lipin (1986), Merkle (1992), Torres-Ruiz et al. (1996), and Maier et al. (1999).

the rhenium and osmium budget of chromitites from the western Bushveld Complex is not accommodated by chromite alone. In this case, the sulfide-bearing interstitial gangue was found to be variably enriched in Re and Os by up to ~20 and ~40 fold, respectively, relative to chromite separates, in agreement with sulfide-chromite partition coefficients of >600 (Re) and >2,000 (Os) measured in this study. The sulfide content of the gangue material was not reported, however, so the precise amount of Re or Os incorporated into the pure sulfide fraction cannot be determined.

As a final point, the textural development of our samples may also offer some insight into the chromite-PGE association. Chromites synthesized in our experiments frequently contain alloy or sulfide inclusions, which vary in size from submicron particles observed as PGE heterogeneities during time-resolved analysis (Fig. 3A) up to a few or more microns as revealed in the exposed surfaces of chromites in sectioned run products (Fig. 1A, B). These textural relationships suggest that chromite nucleation occurs preferentially at the sulfide liquid/silicate melt or alloy/silicate melt interfaces. Thus, our results support a scenario in which the PGE-chromitite association is a consequence of the physical proximity of chromite with PGE-rich phases and not concentration by high-temperature solid solution (see also Hiemstra, 1979; Tredoux et al., 1995). This idea has been previously suggested based on the observation of laurite and Ru-Os-Ir alloy inclusions in chromites from both layered intrusions and ophiolite complexes (e.g., Legendre and Augé, 1986; Talkington and Lipin, 1986; Merkle, 1992; Peck et al., 1992). That these phases were trapped at the magmatic stage is also supported by recent phase equilibrium experiments (Brenan and Andrews, 2001) in which laurite and Ru-Ir-Os alloy were shown to be stable at the chromite liquidus, even under sulfide liquid-undersaturated conditions.

Conclusions

The essential conclusions of this study include the following: (1) our sulfide-silicate melt partition coefficients for Re and the PGE reaffirm the notion that immiscible sulfide melts will dominate the behavior of these elements in sulfide-saturated magmas; (2) D_{Re} is at least a factor of 3 lower than D_{Os}, thus resulting in an increase in the Re/Os ratio of silicate melts derived from partial melting of sulfide-bearing sources or by removal of sulfide liquids at low pressure; and (3) although spinel-silicate melt partition coefficients for the PGE may be of nearly the same magnitude as values measured between sulfide and silicate melt, this similarity may not exist for chromite, given the large minimum sulfide melt-chromite partition coefficients measured in this study. Further confirmation of this latter conclusion, however, awaits a more accurate determination of chromite-silicate melt partitioning at low f_{O_2}. These results suggest that the chromite-PGE association is probably spatial, and not chemical, as high PGE contents in chromitites appear to be related to entrapment of PGM or the presence of interstitial sulfide. Perhaps the largest uncertainty in the entrapment hypothesis is the lack of detailed solubility information for multicomponent PGE alloys and sulfide as functions of f_{O_2}, f_{S_2}, and melt composition. Although solubility information is available for the individual PGE (e.g., O'Neill et al., 1995; Borisov and Palme, 1997; Ertel et al., 1999), only Borisov and Palme (2001) have presented a detailed assessment of the effects of other additives, specifically Fe, whereas it is unknown as to how the individual metal solubilities change by dilution of other PGE. Results of future experiments that address these issues will shed significant light on the origin of PGE-rich accessory phases and the PGE-chromite association.

Acknowledgments

The manuscript benefited from thorough reviews by S-J. Barnes, H. Palme, and an anonymous referee. Discussions with A. J. Naldrett greatly helped to clarify our ideas on PGE behavior in igneous systems. Mike Gorton is thanked for his help in obtaining the INAA analyses. The experimental and analytical work at University of Toronto was funded by a Natural Sciences and Engineering Research Council operating grant OGP 0194228 to J. Brenan. Graduate student support to P. Sattari was provided through an Ontario graduate scholarship. The analytical work at Harvard University was supported by NSF grants (EAR-9506517, EAR-9711008, and EAR-9726058).

March 3, September 17, 2001

REFERENCES

Amossé, J., Dable, P., and Allibert, M., 2000, Thermochemical behaviour of Pt, Ir, Rh and Ru vs. f_{O_2} and f_{S_2} in a basaltic melt. Implications for the differentiation and precipitation of these elements: Mineralogy and Petrology, v. 68, p. 29–62.

Bacuta, G.C., Kay, R.W., Gibbs, A.K., and Bruce, R.L., 1990, Platinum-group element abundance and distribution in chromite deposits of the Acoje block, Zambales Ophiolite Complex, Philippines: Journal of Geochemical Exploration, v. 37, p. 113–145.

Ballhaus, C., and Sylvester, P., 2000, Noble metal enrichment processes in the Merensky reef, Bushveld Complex: Journal of Petrology, v. 41, p. 545–561.

Barnes, S-J., Naldrett, A.J., and Gorton, M.P., 1985, The origin of the fractionation of platinum-group elements in terrestrial magmas: Chemical Geology, v. 53, p. 303–323.

Bezmen, N.I., Asif, M., Brugmann, G.E., Romanenko, I.M., and Naldrett, A.J., 1994, Distribution of Pd, Rh, Ru, Ir, Os, and Au between sulphide and silicate metals: Geochimica et Cosmochimica Acta, v. 58, p. 1251–1260.

Borisiv, A., and Jones, J.H., 2000, An evaluation of Re, as an alternative to Pt, for the 1 bar loop technique: An experimental study at 1400°C: American Mineralogist, v. 84, p. 1528–1534.

Borisov, A., and Palme, H., 1997, Experimental determination of the solubility of Pt in silicate melts: Geochimica et Cosmochimica Acta, v. 61, p. 4349–4357.

——2001, Solubilities of noble metals in Fe-containing silicate melts as derived from experiments in Fe-free systems: American Mineralogist, v. 85, p. 1665–1673.

Brenan, J.M., and Andrews, D., 2001, High temperature stability of laurite and Ru-Os-Ir alloy and their role in PGE fractionation in mafic magmas: Canadian Mineralogist, v. 39, p. 341–360.

Brügmann, A.E., Arndt, N.T., Hofmann, A.W., and Tobschall, H.J., 1987, Noble metal abundances in komatiite suites from Alexo, Ontario, and Gorgona Island, Colombia: Geochimica et Cosmochimica Acta, v. 51, p. 2159–2169.

Capobianco, C.H., and Drake, M., 1990, Partitioning of ruthenium, rhodium, and palladium between spinel and silicate melt and implications for platinum-group element fractionation trends: Geochimica et Cosmochimica Acta, v. 54, p. 869–874.

Capobianco, C.H., Hervig, R.L., and Drake, M., 1994, Experiments on crystal/liquid partitioning of Ru, Rh and Pd for magnetite and hematite solid solutions crystallised from silicate melt: Chemical Geology, v. 113, p. 23–43.

Cawthorn, R.G., 1999, Platinum-group element mineralization in the Bushveld Complex —a critical assessment of geochemical models: South African Journal of Geology, v. 102, p. 268–281.

Crocket, J.H., and MacRae, W.R., 1986, Platinum-group element distribution in komatiitic and tholeiitic volcanic rocks from Munro township, Ontario: Economic Geology, v. 81, p. 1242–1251.

Crocket, J.H., Fleet, M.E., and Stone, W.E., 1992, Experimental partitioning of osmium, iridium and gold between basalt melt and sulfide liquid at 1300°C: Australian Journal of Earth Science, v. 39, p. 427–432.

——1997, Implications of composition for experimental partitioning of platinum-group elements and gold between sulfide liquid and basalt melt: the significance of nickel content: Geochimica et Cosmochimica Acta, v. 61, p. 4139–4149.

Darken, L.S., and Gurry, R.W., 1953, Physical chemistry of metals: New York, McGraw-Hill, 535 p.

Eggins, S.M., Kinsley, L.P.J., and Shelley, J.M.M., 1998, Deposition and element fractionation processes during atmospheric pressure laser sampling for analysis by ICPMS: Applied Surface Science, v. 127–129, p. 278–286.

Ertel, W., O'Neill, H.St.C., Sylvester, P.J., and Dingwell, D.B., 1999, Solubilities of Pt and Rh in a haplobasaltic silicate melt at 1300°C: Geochimica et Cosmochimica Acta, v. 63, p. 2439–2449.

——2001, The solubility of rhenium in silicate melts: Implications for the geochemical properties of rhenium at high temperatures: Geochimica et Cosmochimica Acta, in press.

Fleet, M.E., Crocket, J.H., and Stone, W.E., 1996, Partitioning of platinum-group elements (Os, Ir, Ru, Pt, Pd) and gold between sulphide liquid and basalt melt: Geochimica et Cosmochimica Acta, v. 60, p. 2397–2412.

Hamlyn, P.R., Keays, R.R., Cameron, W.E., Crawford, A.J., and Waldron, M.H., 1985, Precious metals in magnesian low-Ti lavas: Implications for metallogenesis and sulfur saturation in primary magmas: Geochimica et Cosmochimica Acta, v. 49, p. 1797–1811.

Hart, S.R., and Ravizza, G.E., 1996, Os Partitioning between phases in lherzolite and basalt: Geophysical Monograph 95, p. 123–134.

Hiemstra, S. A., 1979, The role of collectors in the formation of the platinum deposits in the Bushveld Complex: Canadian Mineralogist, v. 17, p. 469–482.

Hill, R., and Roeder, P.L., 1974, The crystallisation of spinel from basaltic liquid as a function of oxygen fugacity: Journal of Geology, v. 82, p.709–729.

Holloway, J.R., Pan, V., and Gudmundsson, G., 1992, High pressure fluid-absent melting experiments in the presence of graphite: Oxygen fugacity, ferric/ferrous ratio and dissolved CO_2: European Journal of Mineralogy, v. 4, p. 105–114.

Horn, I., Foley, S.F., Jackson, S.E., and Jenner, G.A., 1994, Experimentally determined partitioning of high field strength- and selected transition elements between spinel and basalt melt: Chemical Geology, v. 117, p. 193–218.

Horn, I., Rudnick, R.L., and McDonough, W.F., 2000, Precise elemental and isotope ratio determination by simultaneous solution nebulisation and laser ablation-ICP-MS: Application to U-Pb geochronology: Chemical Geology, v. 164, p. 281–301.

Jackson, S.E., Longerich, H.P., Dunning, G.R., and Fryer, B.J., 1992, The application of laser ablation microprobe-inductively coupled plasma-mass spectrometry (LAM-ICP-MS) to in situ trace element determinations in minerals: Canadian Mineralogist, v. 30, p. 1049–1064.

Jenner, G.A., Foley, S.F., Jackson, S.E., Green, T.H., Gryer, B.J., and Longerich, H.P., 1993, Determination of partition coefficients for trace elements in high pressure-temperature experimental run products by laser ablation microprobe-inductively coupled plasma-mass spectrometry (LAM-ICP-MS): Geochimica et Cosmochimica Acta, v. 57, p. 5099–5103.

Legendre, O., and Augé, T., 1986, Mineralogy of platinum-group mineral inclusions in chromitites from different ophiolitic complexes, *in* Gallagher, M.J., Ixer, R.A., Neary, C.R., and Prichard, H.M., eds., Metallogeny of the basic and ultrabasic rocks: London, Institute of Mining and Metallurgy, p. 361–375.

Lorand, J.P., Pattou, L., and Gros M., 1998, Fractionation of platinum-group elements and gold in the upper mantle: A detailed study in Pyrenean orogenic lherzolites: Journal of Petrology, v. 40, p. 957–980.

Maier, W.D., and Barnes, S-J., 1999, Platinum-group elements in silicate rocks of the Lower, Critical and Main zones at Union section, western Bushveld Complex: Journal of Petrology, v. 40, p. 1647–1671.

Maier, W.D., Prichard, H.M., Barnes, S-J., and Fisher, P.C., 1999, Compositional variation of laurite at Union section in the western Bushveld Complex: South African Journal of Geology, v. 102, p. 286–292.

McLaren, C.H., and De Villiers, J.P.R., 1982, The platinum-group chemistry and mineralogy of the UG-2 chromitite layer of the Bushveld Complex: Economic Geology, v. 77, p. 1348–1366.

Merkle, R.K.W., 1992, Platinum-group elements in the middle group of chromitite layers at Marikana, western Bushveld Complex: Indications for collection mechanisms and postmagmatic modification: Canadian Journal of Earth Science, v. 29, p. 209–221.

Mitchell, R.H., and Keays, R.R., 1981, Abundance and distribution of gold, palladium and iridium in some spinel and garnet lherzolites: Implications for the nature and origin of precious metal-rich intergranular components in the upper mantle: Geochimica et Cosmochimica Acta, v. 45, p. 2425–2442.

Morgan, J.W., Ganapathy, R., Higuchi, H., and Krahenbuhl, U., 1976, Volatile and siderophile trace elements in anorthositic rocks from Fiskenaesset, West Greenland: Comparison with lunar and meteoric analogues: Geochimica et Cosmochimica Acta, v. 40, p. 861–887.

Murck, B.W., and Campbell, I.H., 1986, The effect of temperature, oxygen fugacity and melt composition on the behavior of chromium in basic and ultrabasic melts: Geochimica et Cosmochimica Acta, v. 50, p. 1871–1887.

Naldrett, A.J., 1981, Platinum-group element deposits. A review: Canadian Institute of Mining and Metallurgy Special Volume 23, p. 197–231.

Okamoto, H., 1992, The Ir-Re (iridium-rhenium) system: Journal of Phase Equilibria, v. 13, p. 649–650.

O'Neill, H.St.C.O., Dingwell, D.B., Borisov, A., Spettel, B., and Palme, H., 1995, Experimental petrochemistry of some high siderophile elements at high temperatures, and some implications for core formation and the mantle's early history: Chemical Geology, v. 120, p. 255–273.

Page, N.J., Cassard, D., and Haffty, J., 1982, Palladium, platinum, rhodium, ruthenium, and iridium in chromitites from the Massif du Sud and Tiebaghi Massif, New Caledonia: ECONOMIC GEOLOGY, v. 77, p. 1571–1577.

Peach, C.L., and Mathez, E.A., 1993, Sulfide melt-silicate distribution coefficients for nickel and iron and implications for the distribution of other chalcophile elements: Geochimica et Cosmochimica Acta, v. 57, p. 3013–3021.

——1996, Constraints on the formation of platinum-group element deposits in igneous rocks: ECONOMIC GEOLOGY, v. 91, p. 439–450.

Peach, C.L., Mathez, E.A., Keays, R.R., and Reeves, S.J., 1994, Experimentally determined sulfide melt-silicate melt partition coefficients for iridium and palladium: Chemical Geology, v. 117, p. 361–377.

Peck, D.C., and Keays, R.R., 1990, Geology, geochemistry, and origin of platinum-group element-chromitite occurrences in the Heazlewood River Complex, Tasmania: ECONOMIC GEOLOGY, v. 85, p. 765–793.

Peck, D.C., Keays, R.R., and Ford, R.J., 1992, Direct crystallisation of refractory platinum-group element alloys from boninitic magmas: Evidence from western Tasmania: Australian Journal of Earth Science, v. 39, p. 373–387.

Righter, K., and Hauri, E.H., 1998, Compatibility of rhenium in garnet during mantle melting and magma genesis: Science, v. 280, p. 1737–1741.

Righter, K., Chesley, J.T., Geist, D., and Ruiz, J., 1998, Behavior of Re during magma fractionation: An example from Volcan Alcedo, Galapagos: Journal of Petrology, v. 39, p. 785–795.

Roeder, P.L., and Reynolds, I., 1991, Crystallisation of chromite and chromium solubility in basaltic melts: Journal of Petrology, v. 32, p. 909–934.

Roy-Barman, M., Wasserburg, G.J., Papanastassiou, D.A., and Chaussidon, M., 1998, Osmium isotopic compositions and Re-Os concentrations in sulfide globules from basaltic glasses: Earth and Planetary Science Letters, v. 154, p. 331–337.

Schoenberg, R., Kruger, F.J., Nagler, T.F., Meisel, T., and Kramers, J., 1999, PGE enrichment in chromitite layers and the Merensky reef of the western Bushveld Complex; a Re-Os and Rb-Sr isotope study: Earth and Planetary Science Letters, v. 172, p. 49–64.

Stockman, H.W., and Hlava, P.F., 1984, Platinum-group minerals in alpine chromitites from southwestern Oregon: ECONOMIC GEOLOGY, v. 79, p. 491–508.

Stone, W.E., Corcket, J.H., and Fleet, M.E., 1990, Partitioning of palladium, iridium, platinum and gold between sulfide liquid and basalt melt at 1200°C: Geochimica et Cosmochimica Acta, v. 54, p. 2341–2344.

Talkington, R.W., and Lipin, B.R., 1986, Platinum-group minerals in chromite seams of the Stillwater Complex, Montana: ECONOMIC GEOLOGY, v. 81, p. 1179–1186.

Tarkian, M., Naidenova, E., and Zhelyaskova-Panayotova, M., 1991, Platinum-group minerals in chromitites from the eastern Rhodope Ultramafic Complex, Bulgaria: Mineralogy and Petrology, v. 44, p. 73–87.

Thy, P., 1983, Spinel minerals in transitional and alkali basaltic glasses from Iceland: Contributions to Mineralogy and Petrology, v. 83, p. 141–149.

Torres-Ruiz, J., Garuti, G.,Gazzotti, M., Gervilla, F., and Fenoll Hach-Ali, P., 1996, Platinum-group minerals in chromitites from the Ojen lherzolite massif (Serrania de Ronda, Betic Cordillera, southern Spain): Mineralogy and Petrology, v. 56, p. 25–50.

Tredoux, M., Lindsay, N.M., Davies, G., and McDonald, I., 1995, The fractionation of platinum-group elements in magmatic systems, with the suggestion of a novel causal mechanism: South African Journal of Geology, v. 98. p. 157–167.

Ulmer, P., and Luth, R.W., 1991, The graphite-COH fluid equilibrium in P, T, f_{O_2} space: An experimental determination to 30 kbar and 1600°C: Contributions to Mineralogy and Petrology, v. 106, p. 265–272.

Von Gruenewaldt, G., and Merkle, R.K.W., 1995, Platinum-group element proportions in chromitites of the Bushveld Complex: Implications for fractionation and magma mixing models: Journal of African Earth Science, v. 21, p. 615–632.

Wallace, P., and Carmicharl, I.S.E., 1992, Sulfur in basaltic magmas: Geochimica et Cosmochimica Acta, v. 56, p. 1863–1874.

Yang, K., Thalhammer, O.A.R., and Seccombe, P.K., 1995, Distribution of platinum-group elements in the great serpentinite belt of New South Wales, eastern Australia: Mineralogy and Petrology, v. 54, p. 191–211.

Zhou, M.-F., Robinson, P.T., Malpas, J., and Li, Z., 1996, Podiform chromitites in the Luobusa ophiolite (southern Tibet): Implications for melt-rock interaction and chromite segregation in the upper mantle: Journal of Petrology, v. 37, p. 3–21.

Zhou, Mei-Fu, Sun Min, Keays, R.R, and Kerrich R.W., 1998, Controls on platinum-group elemental distributions of podiform chromitites: A case study of high-Cr and high-Al chromitites from Chinese orogenic belts: Geochimica et Cosmochimica Acta, v. 62, p. 677–688.